Secondary Swirling Flow in a Bend

Osami KITO

Department of Mechanical Engineering

(Received September 3, 1981)

An analytical study was made on the secondary circulating flows created in a curved duct when a shear type axial flow with a swirling component was introduced in the duct. Depending on the inlet conditions of the flows and configuration of the curved duct, three different types of swirling motions are shown to be created along the curved duct. The results were compared with experiments.

1. Introduction

Flow of a fluid in a curved duct has been the subject of much attention among engineers in relation to flow meters and estimation of flow resistance in pipe line layout, and also among scientists for its physical interest, and many valuable results have been obtained. However, most of these results were for cases in which fully developed flows without swirling components were introduced into a single or a combined bend duct.

In practical cases, however, the flow approaching the bends is not always in a fully developed state, as is indicated in Fig. 1, and the flow pattern in the bends may be considerably different from those for a fully developed flow entrance.

For the case of a shear type flow entrance, Hawthorne[1] and Horlock[2] studied the flow theoretically by considering the vorticity of flow, and showed the occurence of an alternative change of the shear direction along the bend axis. This method, however, is difficult to analyze the entering swirling flow with uniformly distributed or unevently distributed axial velocities, since the streamlines of flow are twisted helically downstream and the angle between the principal normal of the streamline and Bernoulli surface varies considerablly along the line. In principle, this variation was not considered in Hawthorne's analysis, although some correction for this was given in Lakshminarayana's[3] paper.

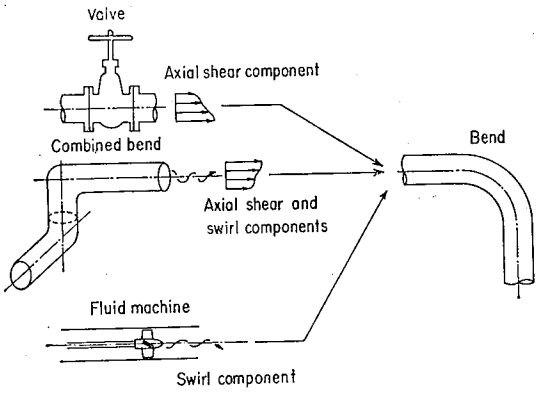

Fig. 1 Uneven flow components introduced in bend

Some detailed experimental studies[4,5] have been performed for these cases, but no theoretical approach has been made.

The present study is concerned with an analytical approach to this secondary flow, and the method involved would be applicable to any type of swirling flow if the velocity profile is approximated by a simple model. Formulation of the flows was performed by use of the momentum theory written in an integral form. The inviscid solutions are firstly given to facilitate understanding the qualitative nature of the flow in a bend. Then the effect of the wall friction is considered to meet quantitative discussion, and comparison with experiments is given.

2. Nomenclature

r, θ, φ	coordinate system, (see Fig. 2)
V_r, V_θ, V_φ	velocity components in r, θ and φ directions, respectively
V_m	mean axial velocity

V_w velocity just outside of wall boundary layer
Ω, Λ, Ξ moment of momentum around pipe axis, P-axis and N-axis, respectively
M_{in}, M_{out} momentums of fluids entering to or issuing from the control surface
Π moment of external force
i, j, k unit vectors directing toward pipe axis, P-axis and N-axis, respectively
C_f friction coefficient
P pressure
r_o radius of pipe
R radius of curvature of bend
α direction of shear (see Fig. 5)
β flow angle next to pipe wall
ε size of sand roughness
ν kinematic viscosity
ξ shear intensity (see Fig. 5)
ω angular velocity of fluid
$\tau_{\theta r}, \tau_{\theta\varphi}$ shearing stresses in r and φdirection in a pipe section
$\tau_{wr}, \tau_{w\varphi}$ shearing stresses in r and φdirection on pipe wall
prime' dimensionless variables
subscript zero values evaluated at the bend entrance section

3. Theory

In this study we assume a steady incompressible flow. The fundamental equations which govern the secondary circulating flows in a curved duct were obtained by considering a change of angular momentum of flows across the curved duct. Figure 2 shows the coordinates system employed in this study; θ is the angular position of a section measured from the bend inlet, and r and φ are the polar coordinates of a point within the section. Figure 3 shows an elementary part of the bend duct whose deflection angle is $\Delta\theta$, and the dotted lines denote a control surface across which a momentum balance of the flow will be considered. The flow entering the section of $\theta = \theta$, the upstream section of the control surface, generally has some angular momentum components around the center line of the section and also around the P- and N-axis, Fig. 4. They are expressed respectively by

$$\Omega(\theta)=\rho\int_0^{r_0}\int_0^{2\pi} V_\varphi V_\theta r^2 d\varphi dr \quad (1)$$

$$\Lambda(\theta)=\rho\int_0^{r_0}\int_0^{2\pi} V_\theta^2 r^2 \cos\varphi d\varphi dr \quad (2)$$

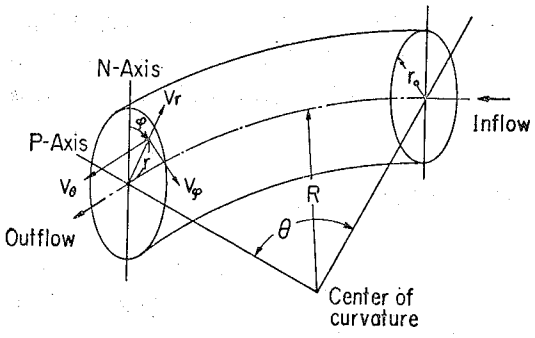

Fig. 2 Coordinates system

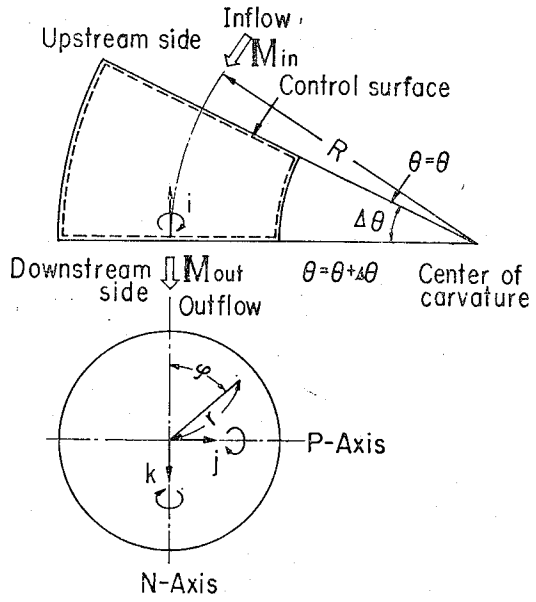

Fig. 3 Small elementary part of bend

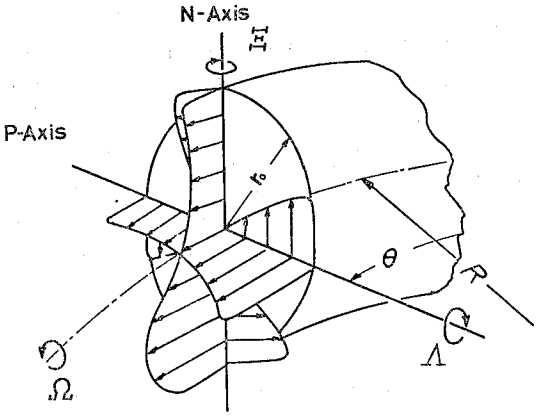

Fig. 4 Definitions of momentums Ω, Λ and Ξ

$$\Xi(\theta)=\rho\int_0^{r_0}\int_0^{2\pi}V_\theta^2 r^2\sin\varphi d\varphi dr \tag{3}$$

From the definition of the momentum, it is evident that the axes of reference are different in up- and downstream sections, since the downstream section is inclined by $\Delta\theta$ to the upstream one.

In order to apply the momentum theory, a unification of the reference axes will be necessary. Let the downstream section $\theta+\Delta\theta$ be this reference section, then the expressions of Eqs. (1), (2) and (3) for the upstream section shoud be changed to those referring to this new reference one. Let unit vectors referred to the center line of the duct and P- and N- axes in the downstream section be i, j and k, respectively, then momentum flowing across the upstream section can be expressed as follow

$$\begin{aligned}Min=&i(\Omega-\Lambda\Delta\theta)\\&+j\{(-\rho R\iint V_\varphi V_\theta\, r\sin\varphi d\varphi dr+\rho R\iint\\&\quad V_r V_\theta r\cos\varphi d\varphi dr+\Omega)\Delta\theta+\Lambda\}\\&+k\{(\rho R\iint V_\varphi V_\theta r\cos\varphi d\varphi dr+\rho R\iint\\&\quad V_r V_\theta r\sin\varphi d\varphi dr)\Delta\theta+\Xi\}\end{aligned} \tag{4}$$

On the other hand, the momentum flux across the downstream section is

$$\begin{aligned}Mout=&\left(\Omega+\frac{d\Omega}{d\theta}\Delta\theta\right)+j\left(\Lambda+\frac{d\Lambda}{d\theta}\Delta\theta\right)\\&+k\left(\Xi+\frac{d\Xi}{d\theta}\Delta\theta\right)\end{aligned} \tag{5}$$

Then the momentum balance across the control surface will be

$$\begin{aligned}Min-Mout=&i\left(-\frac{d\Omega}{d\theta}-\Lambda\right)\Delta\theta+j\left(-\rho R\iint\right.\\&\quad V_\varphi V_\theta r\sin\varphi d\varphi dr\\&+\rho R\iint V_r V_\theta r\cos\varphi d\varphi dr+\Omega-\frac{d\Lambda}{d\theta}\Big)\Delta\theta\\&+k\left(\rho R\iint V_\varphi V_\theta r\cos\varphi d\varphi dr\right.\\&\left.+\rho R\iint V_r V_\theta r\sin\varphi d\varphi dr-\frac{d\Xi}{d\theta}\right)\Delta\theta\end{aligned} \tag{6}$$

If the external force acting on the elementary volume of the fluid is denoted by Π, the following relation will be obtained.

$$\Pi+Min-Mout=0 \tag{7}$$

4. Solution for Fritionless Flow

To see the qualitative nature of the flow, solutions of the flow are found in a frictionless case. Neglecting the effect of the body force, the external force acting on the control surface can be written as

$$\begin{aligned}\Pi=&i\left(-\iint P\cos\varphi r^2 d\varphi\, dr\right)\Delta\theta\\&+j\left(-\iint\frac{\partial P}{\partial\theta}\cos\varphi r^2 d\varphi dr\right)\Delta\theta\\&+k\left(-\iint\frac{\partial P}{\partial\theta}\sin\varphi r^2 d\varphi dr\right)\Delta\theta\end{aligned} \tag{8}$$

if the referring surface is taken to be the downstream one. The pressure acting on the internal surface of the bend, P_w, contributes to the moment of the order of $(\Delta\theta)^2$ and because of its smallness, it can be neglected against the monent given by Eq. (8). For convenience, the following dimensionless expressions will be introduced.

$$\Omega/\rho\pi r_0^3 V_m^2=\Omega',\ \Lambda/\rho\pi r_0^3 V_m^2=\Lambda',$$
$$\Xi/\rho\pi r_0^3 V_m^2=\Xi',\ P/\tfrac{1}{2}\rho V_m^2=P',\ r/r_0=r',\ R/r_0=R',$$
$$V_\varphi/V_m=V_\varphi',\ V_\theta/V'_m=V_\theta',\ V_r/V_m=V_r',$$

In order to solve Eq. (7), the proper assumptions for the velocity distributions will be required. As a flow model in a bend, a forced vortex type flow with a shear type axial velocity as shown in Fig. 5 is assumed as Hawthorne obtained in his analysis, and

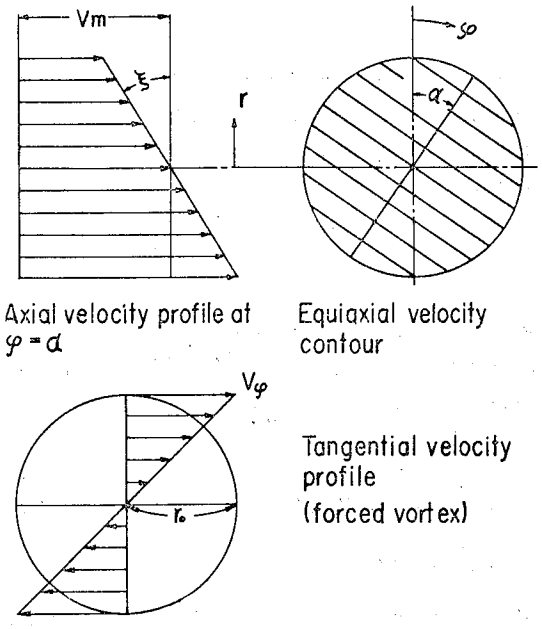

Fig. 5 Assumed velocity distributions in bend

$$\left.\begin{aligned}V_\varphi&=r\omega\\V_\theta&=V_m+r\xi\cos(\varphi-\alpha)\end{aligned}\right\} \tag{9}$$

Except for a special case of a small swirl or weak shear component at the bend inlet, radial velocity V_r is much smaller than V_θ and V_φ, and V_r can be neglected in a qualitative discussion of the flow pattern.

Now, substitution of the relation of Eq. (9) into Eqs. (1), (2) and (3) gives

$$\left.\begin{aligned}\Omega' &= \frac{1}{2}\omega' \\ \Lambda' &= \frac{1}{2}\xi'\cos\alpha \\ \Xi' &= \frac{1}{2}\xi'\sin\alpha\end{aligned}\right\} \tag{10}$$

where $\xi'=\xi/\left(\frac{V_m}{r_o}\right)$ and $\omega'=\omega/\left(\frac{V_m}{r_0}\right)$

Euler's equation of motion in the r- direction

$$V_r\frac{\partial V_r}{\partial r}+\frac{V_\phi}{r}\frac{\partial V_r}{\partial \varphi}+V_z\frac{\partial V_r}{\partial Z}-\frac{V_\varphi^2}{r} - \frac{V_\beta^2\sin\varphi}{R-r\sin\varphi}=-\frac{\partial}{\partial r}\left(\frac{P}{\rho}\right) \tag{11}$$

gives the pressure distribution in the cross section, if the relationship of Eq. (9) is substituted and an integration is performed over the section with respect to r.

Let P_0 be the pressure at the center of the duct section, then

$$\frac{P-P_0}{\rho}=\frac{1}{2}r^2\omega^2+\left(V_m+\frac{R\xi\cos(\varphi-\alpha)}{\sin\varphi}\right)^2\ln\left(1-\frac{r}{R}\sin\varphi\right)+r\xi\cos(\varphi-\alpha)\left(2V_m+\frac{R\xi\cos(\varphi-\alpha}{\sin\varphi}\right)+\frac{1}{2}r^2\xi^2\cos^2(\varphi-\alpha) \tag{12}$$

In the following analsis it is excluded the case in which flow separation occurs in a bend. The separation is avoidable when $R' > 3$, and the term of $\ln(1 - r/R \sin\varphi)$ can be expanded in power series as

$$ln\left(1-\frac{r}{R}\sin\varphi\right)\sim-\frac{r}{R}\sin\varphi-\frac{1}{2}\left(\frac{r}{R}\sin\varphi\right)^2-\frac{1}{3}\left(\frac{r}{R}\sin\varphi\right)^3 \tag{13}$$

if $|r/R \sin\varphi| < 1/3$ is assumed.

Substituting the relations of Eqs. (9), (12) and (13) into Eq. (7), the momentum equation yields

$$\frac{d\Omega'}{d\theta}=-\Lambda' \tag{14}$$

$$\frac{d\Lambda'}{d\theta}=-R'\Omega'\Xi'+\Omega' \tag{15}$$

$$\frac{d\Xi'}{d\theta}=R'\Lambda'\Omega' \tag{16}$$

where small terms including $1/6R'^2$ are all neglected. Equation (14) gives the same formula as Eq. (12) in Hawthorne's paper if we assume the streamline being parallel to the bend curvature and avaraged vorticities over the cross section being introduced.

Elimination of Λ' and Ξ' form above equations gives the following differential equation for Ω' which describes the angular momentum change of fluid along the bend center line

$$\frac{d^2\Omega'}{d\theta^2}+(1-R'K)\Omega'+\frac{1}{2}R'^2\Omega'^3=0 \tag{17}$$

where $K=\frac{1}{2}R'\Omega'^2+\Xi'=\frac{1}{2}R'\Omega_0'^2+\Xi_0'=$ const.

Equation (17) can be solved for a given bend if the inlet conditions, Ω_0', $\left(\frac{d\Omega'}{d\theta}\right)_0=-\Lambda_0'$ and K, are defined. The nonlinear terms in this equation prevent an analytical approach, and recourse should be made to a numerical method.

Before a detailed discussion, the general nature of the differential equation will be given. Eliminating Ξ' from Eqs. (14), (15) and (16) and integrating once the resulting equation with respect to θ, the following expression will be obtained

$$\Lambda'^2+(1-R'K)\Omega'^2+\frac{1}{4}R'^2\Omega'^4=C \tag{18}$$

where C is integral constant.

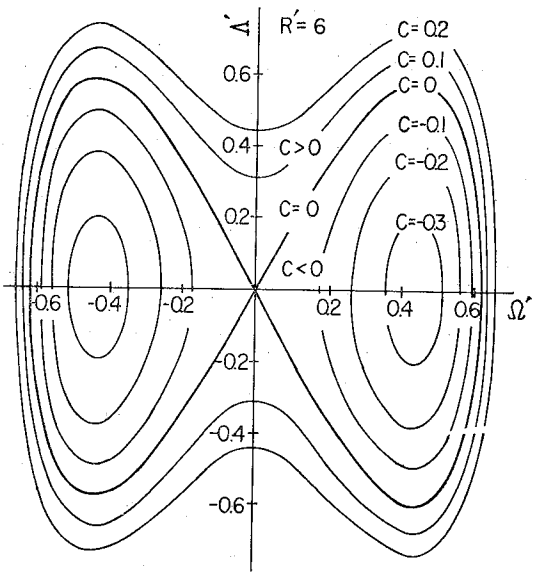

Fig. 6 Relationship between Ω' and Λ'' calculated by Eq. (18) when R' = 6

Figure 6 indicates the relationship of Eq. (18) in the case of $R'=6$. The fundamental difference in the behavior of Ω' occurs depending on the sign of C, namely, $C>0$, $C=0$ and $C<0$. When $C>0$, Ω' changes sinuoulsy and alternative swirl motions occur along the bend. On the other hand, $C < 0$, the sign of Ω' remains the same and gives an unidirectional swirl. Whe $C=0$, all uneven components at the bend inlet disappear gradually. In practice, however, the last case may not

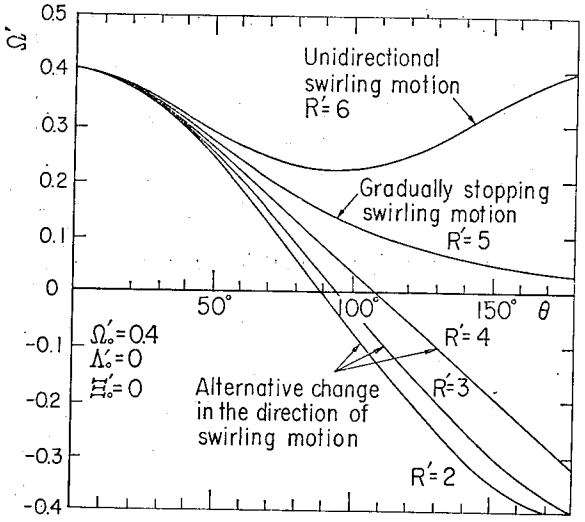

Fig. 7 Change of Ω' along θ when swirling component enters bend

occur, because the effect of wall friction and radial velocity on the swirling flow both of which were neglected in the present discussion become predominantly large in this case.

Equation (17) can be solved numerically by use of a finite difference method for given inlet conditions. Figure 7 indicates the calculated results when an uniformly distributed flow accompanying a forced vortex type swirl component ($\Omega'_0=0.4$, $\Lambda'_0=0$' $\Xi'_0=0$) is introduced to a bend, of which curvature is changed in various values.

5. Solutions for Viscous Flow

Friction forces acting on the control surface are shown in Fig. 8. If the downstream section is taken to be the reference one, the moment of these forces can be expressed by

$$\Pi=i\left\{r_0^2\int\tau_{w\varphi}(R-r_0\sin\varphi)d\varphi-\iint r^2\frac{\partial\tau_{\theta\varphi}}{\partial\vartheta}d\varphi dr\right\}\Delta\theta$$
$$+j\left\{r_0^2\int\tau_{w\theta}\cos\varphi(R-r_0\sin\varphi)d\varphi+\iint\tau_{w\theta}\,r(r-R\sin\varphi)\,d\varphi dr\right.$$
$$\left.+R\iint\tau_{\theta r}\,r\cos\varphi\,d\varphi\,o\vartheta\right\}\Delta\theta+k\left\{r_0^2\int\tau_{w\theta}(R-r_0\sin\varphi)\sin\varphi d\varphi\right.$$
$$\left.+R\iint r\tau_{\theta r}\cos\varphi d\varphi dr+R\iint\tau_{\theta r}\sin\varphi r d\varphi dr\right\}\Delta\theta \qquad (19)$$

In order to simplify the equation, Baker's results[6] for turbulent swirling flows in a duct may be employed. According to him the shearing stress $\tau_{\theta\varphi}$ will satisfy the following inequality relations

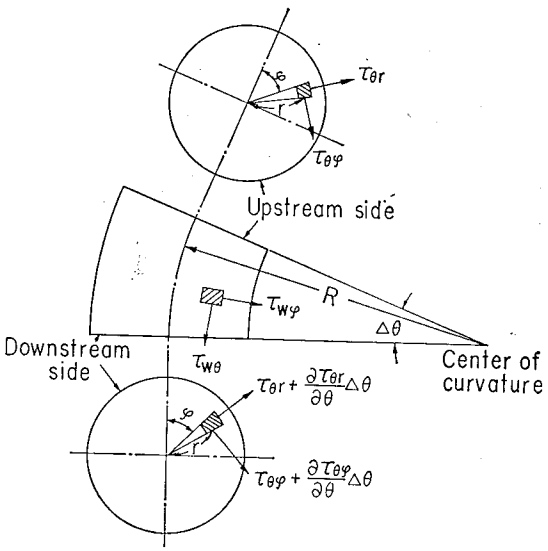

Fig. 8 Shearing stresses on control surface

$$\frac{d\Omega}{d\vartheta}=\frac{d}{d\vartheta}\left\{\rho\iint r^2\,V_\theta V_\varphi\,dr d\varphi\right\}\geqslant\frac{\partial}{\partial\vartheta}\iint r^2\,\tau_{\theta\varphi}\,d\varphi dr$$
$$R\iint\rho\,V_\theta V_\varphi r\sin\varphi d\varphi dr\geqslant R\iint r\,\tau_{\theta\varphi}\sin\varphi d\varphi dr$$
$$\Omega=\rho\iint V_\theta V_\varphi\,r^2 d\varphi dr\geqslant\iint\tau_{\theta\varphi}\,r^2\,d\varphi dr$$
$$R\iint\rho\,V_\theta V_\varphi\,r\cos\varphi d\varphi dr\geqslant R\iint\tau_{\theta\varphi}\,r\cos\varphi d\varphi dr \qquad (20)$$

If the flow angle near the wall is denoted by β, and the wall shear stress in the flow direction by τ_w, Fig. 8, the components of the stresses $\tau_{w\theta}$ and $\tau_{w\varphi}$ can be given by

$$\tau_{w\theta}=\tau_w\cos\beta,\quad \tau_{w\varphi}=\tau_w\sin\beta \qquad (21)$$

With the results of experiments on swirling flows in straight pipes[7], the shear stress in the above equations can be expressed with the resultant flow velocity $V_w=\sqrt{V_{w\theta}^2+V_{w\varphi}^2}$ as

$$\tau_w=\rho C_f\,V_w^2 \qquad (22)$$

where C_f denotes a friction coefficient of the pipe, which depends on reougness of the pipe wall.

If the friction factor for a rough pipe is denoted by λ and that for a smooth pipe by λ_s, C_f can be evaluated by

$$C_f=0.002\lambda/\lambda_s \qquad (23)$$

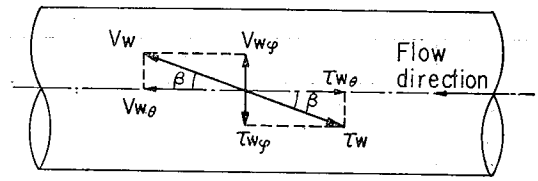

Fig. 9 Direction of flow and shear stress next to pipe wall

When the swirling velocity component $V_{w\varphi}$ is small compared with the axial velocity component $V_{w\theta}$, V_w can be approximated by $V_{w\theta}$, and the following relations can be written;

$$\tau_{w\theta} \fallingdotseq \rho C_f V_{w\theta} V_{w\theta},\ \tau_{w\varphi} \fallingdotseq \rho C_f V_{w\varphi} V_{w\theta} \tag{24}$$

According to the results of experiments in the past, the value of $\tau_{\theta r}$ in one section increases linearly from zero at the center to a maximum value of $\tau_{w\theta}$ at the wall, and the value of $\tau_{\theta r}$ at any radial position of r can be estimated by

$$\tau_{\theta r} \fallingdotseq \tau_{w\varphi\theta}(r/r_0) \tag{25}$$

Using the relationship of Eq. (9) together with Eqs. (24) and (25), the momentum equation of Eq. (7) yields the following three dimensionless equations,

$$\frac{d\Omega'}{d\vartheta} = -4C_f\Omega'(R'-\Xi') - \Lambda' \tag{26}$$

$$\frac{d\Lambda'}{d\vartheta} = -2C_f\Lambda'\left(\frac{8}{3}R' - \Xi'\right) - R'\Omega'\Xi' + \Omega' \tag{27}$$

$$\frac{d\Xi'}{d\vartheta} = -2C_f\left(\frac{8}{3}R'\Xi' - \frac{3}{2}\Xi'^2 - \frac{1}{2}\Lambda'^2\right) + C_f + R'\Omega'\Lambda' \tag{28}$$

The first terms in the right hand side of each equation express the effects of wall friction.

Neglection of the radial velocity component in the above equations may cause a certain amount of error in evaluation of Ξ' in the bend duct, even in the case of a fully developed flow entrance, since secondary flows due to the curved motion in the bend will always develop in the duct. The effect of the radial velocity component can be accounted for briefly in the first approximation if an extra term is added to Eq, (28) as

$$\frac{d\Xi'}{d\vartheta} = -2C_f\left(\frac{8}{3}R'\Xi' - \frac{2}{3}\Xi'^2 - \frac{1}{2}\Lambda'^2\right) + C_f + R'\Omega'\Lambda' + A \tag{29}$$

The value of A in this equation may be determined so as to accord with the experiment in fully developed flows, but here we use the values of Table 1 given for some of the bend ducts which can be calucalted from simplified potential flow model. Numerical solutions of Eqs. (26), (27) and (29) give the characteristic changes in Ω' in curved ducts. Figure 10 shows the relationship of Ω' and

Table 1

R/r_0	$0° < \theta < 45°$	$45° < \theta < 180°$
3	0.253	−0.0845
4	0.173	−0.0576
5	0.134	−0.0446
6	0.114	−0.038

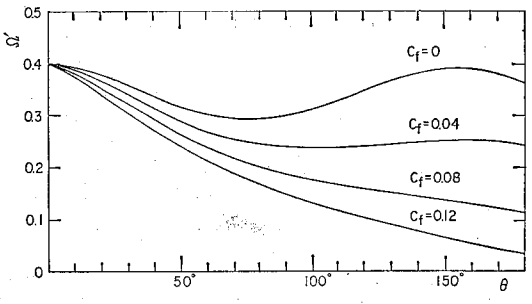

Fig. 10 Change of swirl intensity along θ when swirling component enters bend

θ when a uniform axial velocity with a swirling component introduced to a bend of $R/r_0=6$. The friction factors of C_f used here are those which cover the ranges in practical use. In the case of $C_f=0$, namely a frictionless case, the swirling intensity Ω' changes sinuously as θ increases and shows no decay. If $C_f>0$, the decay in Ω' along the duct appears and wavy change of Ω' becomes weak.

6. Comparison of Numerical Solutions with Experiments

The results of numerical solutions of the equations given in the previous section are confirmed by experiments.

The present author measured the flow in a single bend when swirling flows with various intensities were introduced, and the effects of wall rougness on the secondary swirling motions were also studied. The experimental equipment is shown in Fig. 11. The bend duct was made of brass and had a hydraulically smooth surface. Its inside diameter was 50.9mm and the bend radius $R/r_0 = 6$. To check the effects of wall friction the surface of the wall was roughened artificially with sands. Velocity distributions were measured at five sections of $\theta=0°$, 90°, 135° and 180°, respectively, by use of a cylindrical Pitot tube, when $Re=\frac{2Vmr_0}{\nu}=10^5$. In each section, the Pitot tube was traversed in four directions; along P- and N-axes and along its bisectors. The momentum fluxes were obtained by substituting measured values in Eqs. (1), (2) and (3) and integrating it numerically.

Experimental uncertainties for the measured values are estimated as flollow

Limit if θ; $\pm$ 1.5°

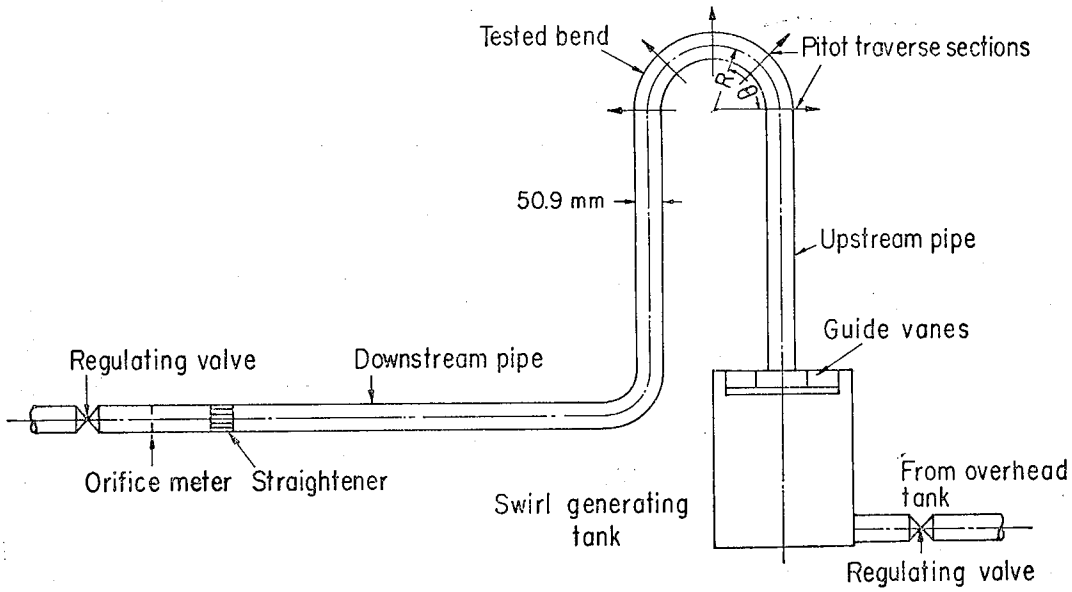

Fig. 11 Experimental apparatus

Limit of V_m: $\pm$ 3% (at about V_m= 1.7m/s)
Limit of V_θ: $\pm$ 0.03V_m(except wall region)
Limit of $V\varphi$: $\pm$ 0.02 V_m(except wall region)

Uncertainties concerning to the values of Ω' Λ' and Ξ' are difficult to estimate because numerical integrations of Eqs. (1), (2) and (3) were performed using limited point measurements (108 points in one section) instead of infinite number of them, but many repeated measurements make possible to offer the accurate values of Ω', Λ' and Ξ' within the error of $\pm$ 0.015.

Figure 12 shows the experimental results of momentum change along the bend when an uniform axial flow with a swirling component enters the bend. This inlet condition corresponds to the case of C = $-$ 0.059 in Eq. (18), which gives an unidirectional swirling flow in the bend. The dashed lines indicate the calculated results for the same inlet conditions as the experiments. The agreement is satisfactory for Ω' and Λ' but only qualitative for Ξ'.

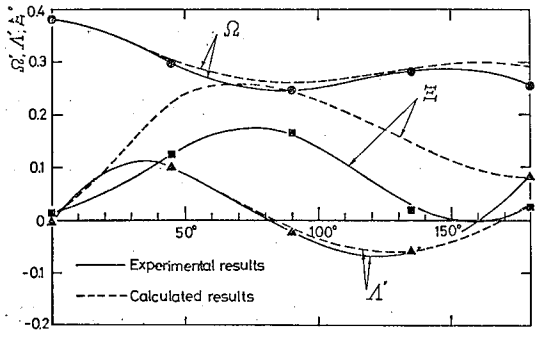

Fig. 12 Comparison of theoretical and experimental results in case when a nearly uniform axial flow ($\Lambda_0' = -0.003$, $\Xi_0' = 0.015$) with a swirling component ($\Omega_0' = 0.382$) enters bend of $R/r_0 = 6$

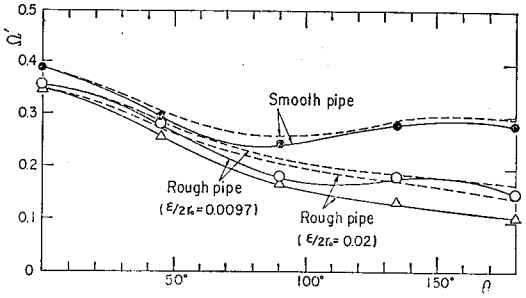

Fig. 13 Comparison of experimental results with theoretical ones when a swirl component is introduced to bend with different wall roughness ($\Omega_0' = 0.35 \sim 0.39$)

Figure 13 exhibits the effect of wall roughness on secondary swirling component. The inlet conditions are the same as the case of Fig. 12, except for a small difference in Ω_0'. The secondary swirling becomes smaller as the wall is roughened as expected from Eq. (26). The calculated results, dashed lines, deviate somewhat from experiment in rough wall.

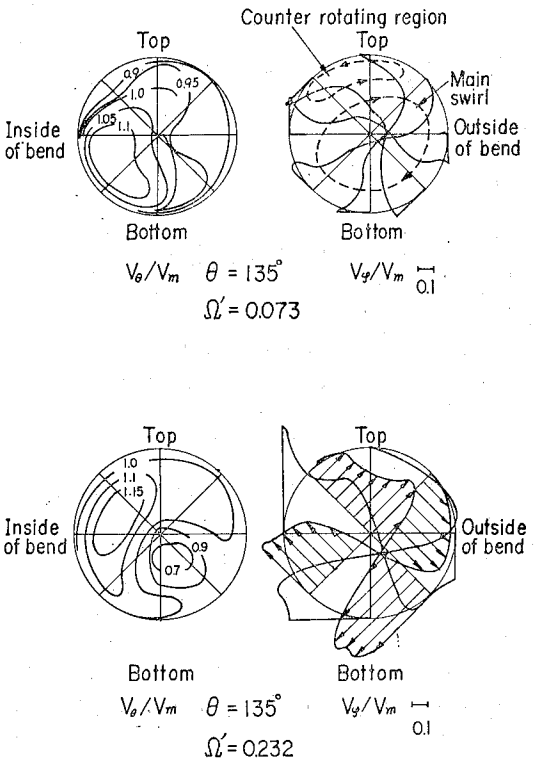

Fig. 14 Velocity distributions in bend when uniform axial flow with swirling component (Ω_0' = 0.306, 0.156) enters a bend of $R/r_0 = 6$

7. Distributions of Velocities

Figure 14 shows the velocity distributions measured at the section of θ=135° in the bend of R/r_0=6. When Ω'=0.073 (a weak swirl), the tangential velocity shows approximately a forced vortex type profile except in the wall region, where a vortex pair with the opposite sign is seen to be created as in an ordinary secondary flow in a bend. The occurence of the vortex pair will bring about some discrepancy in the theory and experiments, especially in the case of a weak swirl. When the swirl intensity is increased to $\Omega' = 0.232$, a free vortex type profile is developed in the tangential velocity component, and the effect of the secondary flow due the duct curvature on the total flow pattern becomes less. The axial velocity profiels exhibit a shear flow type motion as was assumed, but different concave pattern appears as the swirl is increased.

Although the assumed velocity profile are not exactly the same with the measured ones, they give fairly good agreement in the values of momentum except for a case of weak swirl. Calculation with the assumpation of a forced-free vortex with concave axial velocity as seen in the measured flow gives no substantial change in the estimation of Ω' from that of Eq. (9).

8. Concluding Remarks

A secondary swirling flow in a bend caused by uneven inlet velocity distributions was described theoretically, and the results were compared with those from experiments. The following are the main conclusions.

(1) The behavior of the secondary swirling flow can be classified into three flow types, depending on the inlet conditions and the configurations of the duct curvature;

(a) Flow with a unidirectional swirl

(b) Flow with an alternative directional swirl

(c) Flow with a gradual terminating swirl, although it may not appear in practical cases

(2) Change of the swirl intensity is generally observed along the axis of the curved duct. The occurence of this change can be explained on the basis of the conservation law of the inlet momentum of fluids around the duct axis.

(3) Friction forces on the duct wall have a damping effect on secondary swirling motions.

The author would like to show his thanks to professor M. Murakami of Nagoya university for his kind advice and to Mr. H. Yoshida for his collaboration in experiments.

References

(1) Hwthorne, W.R., *Proc. Roy. Soc. Lond.*, Ser.A, 206–1086 (1951–5), 374.

(2) Horlock, J.H., *Proc. Roy. Soc. Lond.*, Ser. A, 234–1198(1956–2), 335.

(3) Lakshminarayana, B., and Horlock, J.H., *J. Basic Engng.*, (1967–3), 191.

(4) Shimuzu, Y., and Sugino, K., *Bull. JSME*, 23–183 (1980–9), 1443.

(5) Murakami, M., and Shimizu, Y., *Bull. JSME*, 21–157(1978–7), 1144.

(6) Baker, D.W., *Diss.*, Univ. Marlyand, 1967.

(7) Murakami, M., and et al., *Bull. JSME*, 19–128 (1976–2), 118.